Measurements of ^{27}Al(γ, n) reaction using quasi-monoenergetic γ beams from 13.2 MeV to 21.7 MeV at SLEGS*

Pu Jiao,[1,2,†] Zi-Rui Hao,[2,†] Qian-Kun Sun,[3,4] Long-Xiang Liu,[2] Hang-Hua Xu,[2] Yue Zhang,[2] Meng-Die Zhou,[1,2] Zhi-Cai Li,[5,2] Wen Luo,[5] Yu-Xuan Yang,[6,3] Sheng Jin,[3,4] Kai-Jie Chen,[7,3] Shan Ye,[8,2] Zhen-Wei Wang,[3,4] Yu-Ting Wang,[1] Hui-Ling Wei,[1] Yao Fu,[3] Kun Yu,[9,10] Hong-Wei Wang,[2,3,4] Gong-Tao Fan,[2,3,4,‡] and Chun-Wang Ma[1,11,§]

[1]*College of Physics, Centre for Theoretical Physics, Henan Normal University, Xinxiang 453007, China*
[2]*Shanghai Advanced Research Institute, Chinese Academy of Sciences, Shanghai 201204, China*
[3]*Shanghai Institute of Applied Physics, Chinese Academy of Sciences, Shanghai 201800, China*
[4]*University of Chinese Academy of Science, Beijing 100080, China*
[5]*School of Nuclear Science and Technology, University of South China, Hengyang 421001, China*
[6]*School of Physics and Microelectronics, Zhengzhou University, Zhengzhou 450001, China*
[7]*ShanghaiTech University, Shanghai 201210, China*
[8]*China Institute of Atomic Energy, Beijing, 102413, China*
[9]*College of Physics, Henan Normal University, Xinxiang 453007, China*
[10]*Henan Key Laboratory of Infrared Material & Spectrum Measures and Applications, Henan Normal University, Xinxiang 453007, China*
[11]*Institute of Nuclear Science and Technology, Henan Academy of Sciences, Zhengzhou 450046, China*

The accurate photoneutron cross section of the ^{27}Al nucleus has an important impact on clarifying the differences in existing experimental data and improving the precision of the calculation of the nuclear reaction rate of ^{26}Al in nuclear astrophysics. The photoneutron cross sections for the ^{27}Al(γ, n)^{26}Al reaction, within the neutron separation energy of 13.2 to 21.7 MeV, have been meticulously measured with a new flat efficiency detector (FED) array at the Shanghai Laser-Electron Gamma Source (SLEGS). The uncertainty of the data are controlled below 4% throughout the process and inconsistency between the present data and the existing data from different sources of gamma, as well as the TENDL-2021 data, is discussed in detail. These discussions provide a reference and help solve the inconsistency of the data of the ^{27}Al(γ, n)^{26}Al cross section and improve the related theoretical calculation.

Keywords: photoneutron cross section, flat efficiency detector, laser Compton scattering, γ rays, SLEGS

I. INTRODUCTION

The investigation of giant dipole resonance (GDR) [1] in nuclear physics during the 1960s to 1980s involved active measurements of photoneutron cross sections. Currently, comprehensive documentation of the GDR data is available on various web platforms [2]. Specifically, research on GDR photoreaction was facilitated by the utilization of quasi-monochromatic γ rays generated through positron annihilation in flight (PAIF) at two prominent research institutions, namely Saclay (France) and Lawrence Livermore National Laboratory (USA) [3]. Research on low-energy photonuclear reactions has been revitalized since 2000, due not only to advancements in the field of low-energy electric dipole strength (pygmy dipole resonance, PDR) [4], but also to studies on the origins of elemental nucleon synthesis in nuclear astrophysics [5, 6]. The development of the new γ-ray source known as laser Compton Scattering (LCS) opens the new technique to the systematic study of the γ induced nuclear reaction with monoenergetic incident energy [7]. This resurgence has been further facilitated by the application in institutions and facilities such as the National Institute of Advanced Industrial Science and Technology (AIST) [9–11], NewSUBARU BL01 [12–14], and HIγS [15, 16].

The ^{27}Al(γ, n)^{26}Al reaction plays a crucial role in astrophysical processes, particularly within high-temperature and high-density environments such as the core of stars, supernova explosions, and other high-energy events [8]. This reaction is triggered by the absorption of high-energy γ-rays by the ^{27}Al nucleus, bridging the gap between nuclear physics and astrophysics. Using these γ-rays, the reaction enables the production and transformation of nuclei and offers valuable insights into the evolution of the universe, the intricacies of nuclear reaction networks, and the mechanisms involved in energy transfer within astrophysical environments. Large differences among measured ^{27}Al(γ, n)^{26}Al reactions has been found due to the techniques for measurement or data analysis, making it difficult to accurately understand the underlying physical mechanisms.

Traditional methods for measuring the cross sections of ^{27}Al(γ, n)^{26}Al, such as bremsstrahlung [17, 18] unfolding techniques or in-flight annihilation of monochromatic positrons, often produce conflicting results with discrepancies of 20%-50% [19]. The former method is prone to systematic errors due to mathematical unfolding, while the latter suffers from intensity calibration issues of the photon beam, resulting in systematic errors of about 7% even at peak values of the GDR. In contrast, the LCS γ rays for ^{27}Al(γ, n)^{26}Al measurements offer advantages, as they are free of low-energy tail effects. In this study, the energy dependence of the ^{27}Al(γ, n)^{26}Al cross sections was systematically mea-

* Supported by the National key R&D program (No. *2023YFA1606901*, No. *2022YFA1602404*, the National Natural Science Foundation of China (Grant Nos. *12375123* and *12388102*), and the Natural Science Foundation of Henan Province (No. *242300422048*).

† Co first authors.
‡ Corresponding author.Gong-Tao Fan, fangt@sari.ac.cn
§ Corresponding author.Chun-Wang Ma, machunwang@126.com

sured using the LCS γ-ray method. Compared to sources such as bremsstrahlung, the derivation of monoenergetic cross sections using an LCS source is relatively complex and requires more experimental time. However, the methods and data reduction techniques employed have been improved and the results have been compared with previous measurement results. This comparison highlights significant discrepancies and uncertainties associated with each method.

II. EXPERIMENT

A schematic illustration of SLEGS [20] and the corresponding experimental setup are presented in Fig. 1. After traversal through the collimation system, the LCS γ-ray beams strike the metallic ^{27}Al targets which are located at the central focus of the Flat Efficiency Detector (FED).

A. Brief introduction to SLEGS beamline

The SLEGS beamline [20–26] at the Shanghai Synchrotron Radiation Facility (SSRF) provides quasi-monochromatic γ rays with maximum scattering energies (E_γ) from 0.66 to 21.7 MeV. This beamline utilizes the inverse Compton scattering technology, which involves the collision of photons from a 10,640 nm, 100 W CO_2 laser with 3.5 GeV electrons in the storage ring of the SSRF. The γ beam energy is tuned in the slant-scattering mode with a minimum step of 10 keV, allowing the cross section to be mapped much more precisely in contrast to the γ-ray beam under backward scattering at AIST [7] and NewSUBARU BL01 beamline [27].

The experiment was carried out using the SSRF storage ring, which was operated in top-up mode with a beam current of (160-210) mA and an energy of 3.5 GeV. A CO_2 laser, delivering average (5-20)W of power with a frequency of 1 kHz and a pulse width of 50 μs, was employed to generate γ-rays. The γ-rays were collimated using the C5T2 double collimator. Changing the interaction angle from 102° to 180°, γ rays with theoretical energies ranging from 13.16 to 21.73 MeV were produced. A total of 38 energy points of the ^{27}Al(γ, n)^{26}Al reaction cross sections were measured within this energy range. The incident gamma spectrum on the detector can be derived using the direct unfolding method, as outlined in reference [28–30]. Figure 2 illustrates the detector response spectrum (blue dash-dotted line) and the unfolded spectra at the slant-scattering angles of 103°, 124°, and 155° (red dashed lines). The black line represents the reconstructed spectrum obtained by convolving the incident gamma spectrum with the simulated detector response matrix [31], which shows good agreement with the measured spectrum. The theoretical Compton edge energies for the interactions at 103°, 124°, and 155° are 13.37, 16.96, and 20.71 MeV, respectively. These values correspond closely to the energies at half-peak height on the high-energy side of the incident gamma spectrum.

B. Al Target

The aluminum (Al) target consists of five 10 mm in diameter and 25 mm in thickness of ^{27}Al isotope, 100% abundance and 99.99% purity. Detailed specifications can be found in Table 1

Table 1. Elemental components (in ppm) of the ^{27}Al target used in experiments.

Mn	Mg	Si	Ti	V	Cr
0.13	1.35	2.87	0.26	0.24	0.20
Fe	Ni	Cu	Zn	Ga	
3.06	0.08	3.19	0.26	0.34	

Total chemical impurities ^{27}Al > 99.99 %

Physical form

Weight	Diameter	Total thickness	Density
5.21g	10.00mm	24.74mm	2.68g/cm^3

The targets were placed in a polythene sample holder with a 10 mm diameter window. Considering that the size of the LCS γ-ray beams was approximately 4 mm in diameter at the target position, the 10 mm diameter of the window was sufficient for the target to be measured without the influence of neutrons from polythene.

C. Measurements

Details of the measurement and analysis are described in Ref. [32], and are therefore only briefly described here. Items measured to decide the cross sections were the energy distribution and the flux of LCS γ rays irradiating the sample, and the number of neutrons due to (γ, n) reactions. The energy distribution of LCS γ rays was measured by a BGO detector and was deduced by unfolding the charge integration spectrum using the BGO response functions.

In the FED system, proportional counters are embedded in moderators, such as paraffin or polyethylene, where emitted neutrons of the reaction are thermalized. The large neutron capture cross section of ^{3}He for thermal neutrons makes it an ideal medium for neutron measurement. The flat efficiency response is achieved by optimizing the position of the ^{3}He counters in the moderator. Usually, the ^{3}He counters are distributed in concentric rings. The efficiency of the inner ring is the highest, but decreases rapidly as neutron energy increases. The outer rings are responsible for compensating the loss of inner ring efficiency at high incident neutron energies, so that the total detector efficiency varies little over a wide energy range. In NewSUBARU [35], the ^{3}He FED composed of ^{3}He proportional counters has been shown to be an effective tool for studying the photoneutron cross section.

A new ^{3}He FED device has been developed at the SLEGS station [32]. Figure 3 shows the structure of the FED system and the device features 26 sets of ^{3}He proportional counters integrated within a polyethylene moderator. These counters are organized into three concentric rings located at specific distances from the central beam axis, measuring 65, 110, and

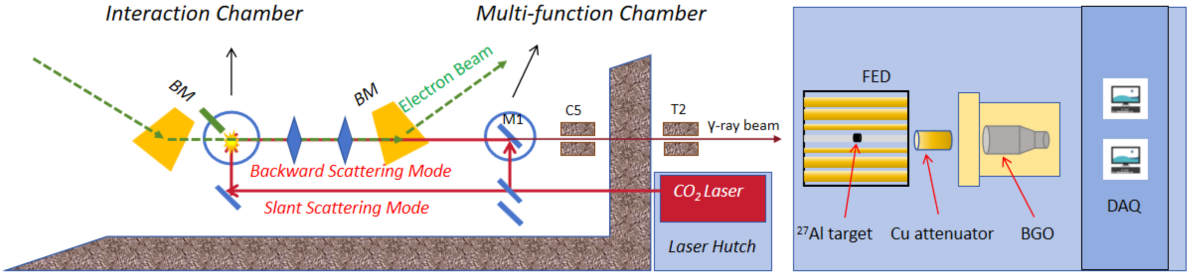

Fig. 1. (Color online) The setup of SLEGS. A set of two collimators of 5 mm (C5) and 2 mm (T2) aperture was used for the ^{27}Al(γ, n)^{26}Al in experiment.

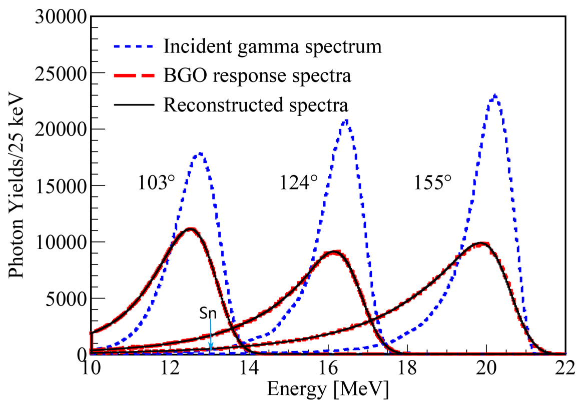

Fig. 2. (Color online) A typical γ spectrum obtained by BGO detector (red dash line) and the corresponding unfolded γ spectrum (blue dash-dot line). The reconstructed spectrum is shown as black line. The spectrum is measured with C5T2.

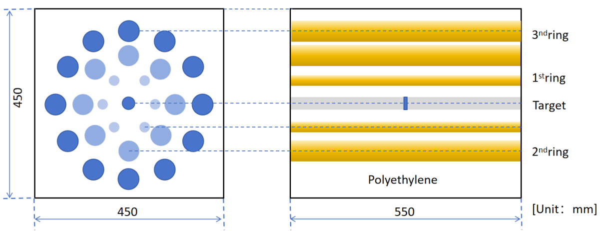

Fig. 3. (Color online) Structure of the FED. The left and right panels denote the front view and the lateral profile of FED.

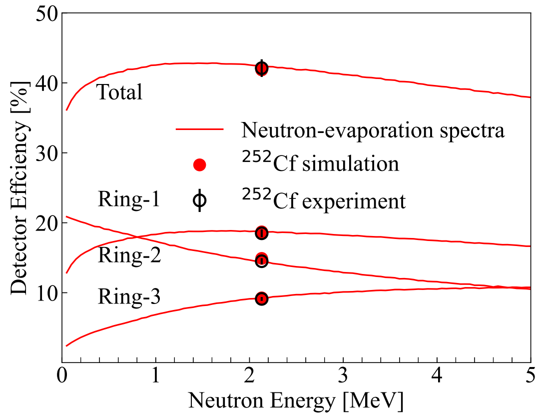

Fig. 4. (Color online) The total detector efficiency and the efficiencies of individual rings. The detector efficiency curves were simulated by neutron-evaporation spectra and monochromatic neutrons. The red dots are given by the neutron spectrum described by the Maxwell-Boltzmann distribution, at the average neutron energy (T = 1.42 MeV) of ^{252}Cf [33].

175 mm, respectively. The moderator encompasses a tunnel designed to facilitate the passage of the gamma beam, with the target situated at the central point of the three rings. The sensitive volumes of the ^{3}He proportional counters are cylindrical in shape, each with a consistent length of 500 mm and pressurized with 2 atm of ^{3}He gas. The counters in Ring-1 (inner ring) have the diameter of 1 inch, while those in Ring-2 (middle ring) and Ring-3 (outer ring) have the diameter of 2 inch. The counter is made of thin stainless steel walls, with low background, strong γ resistance, and good pressure resistance. The size of the inner polyethylene moderator is 450 mm $\times$ 450 mm $\times$ 550 mm along the beam direction. In order to further attenuate environmental neutron interference, the 2 mm thick Cadmium(Cd) sheets are employed to cover all six surfaces of the moderator. Finally, the inner moderator and the cadmium sheets are sealed together using additional polyethylene plates. The ^{3}He proportional counters are powered by the CAEN SY4527LC crate, ensuring a minimal high voltage deviation of no more than 1 V. The initial signals generated from the ^{3}He counters are channeled to preamplifiers. These signals are then collected and preprocessed using the Mesytec MDPP-16, a digital pulse processor renowned for its high time and amplitude resolution, which enables the generation of precise reconstructed waveforms. For data acquisition, the MVME DAQ system was employed. Figure 4 presents the simulated efficiency curve obtained using Geant4, based on the described detector construction. The total detector efficiency exhibits an increasing trend from 35.6% at 50 keV to 42.3% at 1.65 MeV, fol-

lowed by a gradual decline to 40.7% at 3 MeV for the average neutron energy. In particular, the efficiency calibrated using a ^{252}Cf source resulted in a value of 42.1 $\pm$ 1.3% at 2.13 MeV, representing the average energy of the neutron spectrum ^{252}Cf, and is indicated on the curve. Furthermore, the uncertainty of the efficiency curve was assessed by varying the density of the moderator, the gas pressure, and the sensitive volume of the counters ^{3}He. Using the efficiency curve, a rough estimate of the detector efficiency can be derived from the range of the incident neutron spectrum. However, for a precise characterization of the neutron detector efficiency with specific energy profiles, the calculation of the weighted average efficiency is necessary.

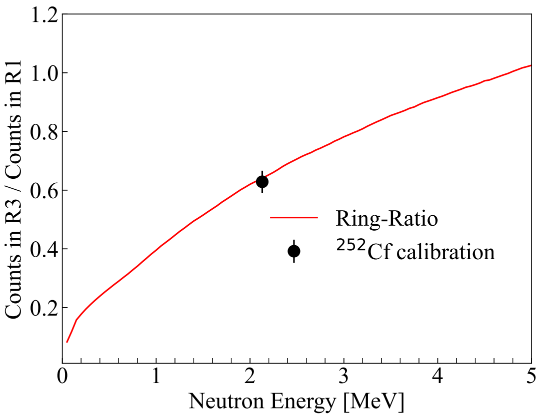

Fig. 5. (Color online) The Ring-Ratio curve of the FED array.

The Ring Ratio technique, which exploits the energy dependence of the ring ratio, was originally developed by Berman *et al* [5, 34, 35]. Figure 5 presents the Geant4 simulations illustrating the Ring Ratios as a function of neutron energy.

III. ANALYSIS AND DISCUSSION

A. Monochromatic Approximation

The cross section in the monochromatic approximation is given by

$$\int_{S_n}^{E_{max}} n_\gamma(E)\sigma(E)dE = \frac{N_n}{N_\gamma N_t \xi \epsilon_n}. \quad (1)$$

Whereas,$n_\gamma(E)$, the energy distribution of the LCS γ-ray beams, is normalized to unity in the energy region of integration. $\sigma(E)$ represents the photoneutron cross section, N_n the number of detected neutrons. N_t denotes the number of target nuclei per unit area, while N_γ represents the number of γ particles incident to the target with energies above the neutron threshold. The correction factor for a thick target measurement is expressed as $\xi = (1 - e^{\mu t})/\mu t$, where μ denotes the linear attenuation coefficient of photons in the target material and t represents the thickness of the target. Moreover, the symbol ϵ_n represents the neutron detection efficiency.

$$\sigma^{E_{max}}_{(\gamma,n)} = \frac{N_n}{N_\gamma N_t \xi \epsilon_n}. \quad (2)$$

Assuming E_{max} represents the energy of the LCS γ-ray beams, the photoneutron cross sections are obtained at the energy in the monochromatic approximation by Eq. (2). The γ beam was collimated to 2 mm in diameter with a three-hole collimator. However, due to the energy dispersion of the LCS γ-ray beams (see Fig. 2), the monochromatic approximation is inadequate for determining photoneutron cross sections.

In the experiment, the laser pulse period is 1000 μs, consisting of a 50 μs laser on time and a 950 μs off time. This pulse period facilitates the process of inverse Compton scattering between the laser and electron beam, resulting in the production of γ-rays with inherent time broadening. Consequently, the neutrons generated by the interaction with the experimental target exhibit time broadening as well. To accurately count the number of neutrons, the FED array is employed, which involves identifying the flat efficiency zone and measuring neutron counts within this region. However, the flat efficiency zone varies with neutron energy as well as other factors such as the size of each ring and ambient conditions like counter's gas pressure. Therefore, it is necessary to determine the flat efficiency region for each ring at different energy levels and use the median method to establish the optimal efficiency point. This strategy ensures a more reasonable statistical analysis of neutron counts.

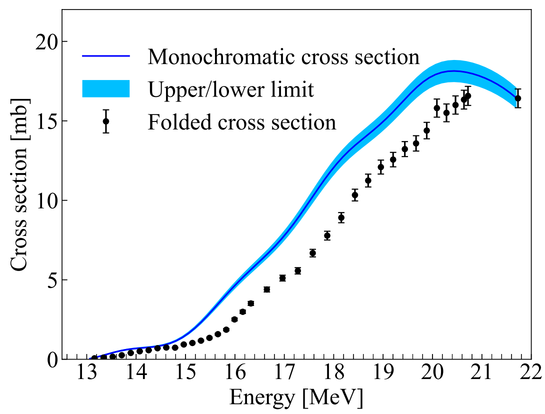

Fig. 6. (Color online) Cross sections of ^{27}Al(γ, n)^{26}Al measured at SLEGS. The dots are the folded cross section and the line with shaded area is the unfolded (monochromatic) cross section.

B. Unfolding Photoneutron Cross Sections

By approximating the integral in Eq. (1) with a summation for each γ-beam profile, we are able to express the unfolding problem as a set of linear equations. The unknown cross

section σ can be obtained by solving the equations for the system $\sigma_f = \mathbf{D}\sigma$, where σ_f represents the folded cross section with the beam profile $\mathbf{D}$. The approach solves the unfolding problem by formulating it as a linear algebra problem, which is

$$\begin{pmatrix} \sigma_1 \\ \sigma_2 \\ \vdots \\ \sigma_N \end{pmatrix}_{\mathrm{f}} = \begin{pmatrix} D_{11} & D_{12} & \cdots & D_{1M} \\ D_{21} & D_{22} & \cdots & D_{2M} \\ \vdots & \vdots & \ddots & \vdots \\ D_{N1} & D_{N2} & \cdots & D_{NM} \end{pmatrix} \begin{pmatrix} \sigma_1 \\ \sigma_2 \\ \vdots \\ \vdots \\ \sigma_M \end{pmatrix}. \quad (3)$$

The matrix $\mathbf{D}$ is composed of normalized incident gamma energy distributions from S_n to E_{max} at discrete beam energies (E_γ). The system of linear equations presented in Eq. (3) is underdetermined, which makes it not feasible to directly extract the true vector σ by matrix inversion. To determine σ, the folding iteration method [36, 37] was summarized in the following.

The start of the process is from the zero-*th* iteration of a constant trial function σ_0. This initial vector is multiplied with $\mathbf{D}$, and the zero-*th* folded vector is obtained $\sigma_f^0 = \mathbf{D}\sigma^0$. The next trial input function is denoted as σ_1. It is proposed by adding the difference between the experimentally measured spectrum σ_{exp} and the folded spectrum σ_f^0 to $\mathbf{D}\sigma^0$. To enable the addition of folded and input vectors, a spline interpolation is initially performed on the folded vector to ensure that both vectors have matching dimensions. The new input vector is,

$$\sigma^1 = \sigma^0 + (\sigma_{exp} - \sigma_f^0). \quad (4)$$

The above steps are iterated i times, which yields

$$\sigma_f^i = \mathbf{D}\sigma^i, \quad (5)$$

and

$$\sigma^{i+1} = \sigma^i + (\sigma_{exp} - \sigma_f^i). \quad (6)$$

The updated input vector is determined iteratively until convergence is attained. The convergence criterion is met when σ_f^{i+1} approximates σ_{exp} within the statistical error limits. Convergence is quantitatively assessed by computing the reduced χ^2 between σ_f^{i+1} and σ_{exp} at the end of each iteration. Typically, around three iterations are adequate for achieving convergence, characterized by a reduced χ^2 value approaching 1.

The monochromatic cross sections of the ^{27}Al(γ, n)^{26}Al reaction are derived using the unfolding iteration method. Fig. 6 compares the quasimonochromatic and monochromatic cross sections for ^{27}Al. Statistical uncertainties are attributed solely to neutron counts, as the high number of γ-ray counts results in negligible uncertainties. Total uncertainty encompasses statistical, systematic, and methodological components. The total uncertainty estimate for ^{27}Al(γ, n)^{26}Al is less than 4%, except for data points that correspond to lower cross-sectional values and an energy of 21.7 MeV. The cross sections for the SLEGS experiment are comparable or even higher quality than some of the datasets in the EXFOR database. Conclusions on systematic uncertainties are as follows.

- The total uncertainty in the efficiency of the neutron detector is 3.0%.
- The uncertainty in the reconstructed incident energy spectrum due to the external copper attenuator and the target is 0.50%.
- The uncertainty in the target thickness is estimated to be less than 0.10%.

The uncertainties associated with data processing for cross-sectional calculations are summarized below.

- The neutron count extraction algorithm introduces an uncertainty of approximately 2%.
- The BGO detectors exhibit 100% efficiency; when combined with the modeled BGO reaction matrix, the overall uncertainty is approximately 1%.

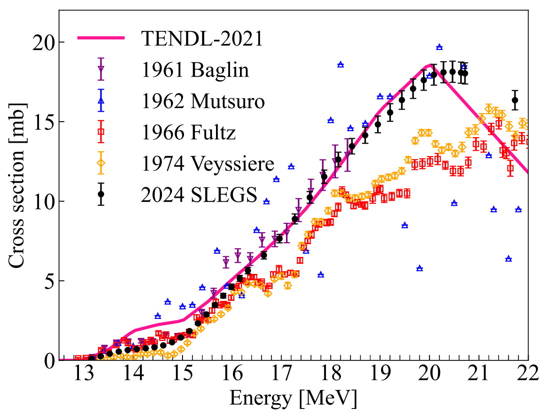

Fig. 7. (Color online) The measured cross section for ^{27}Al(γ, n)^{26}Al (solid circles) at SLEGS and comparison with existing data. The solid line denotes the TENDL-2021 evaluation. Results measured with bremsstrahlung γ rays (Baglin 1961 and Mutsuro 1962) are shown by filled inverted triangles and filled triangles, respectively. Results measured with PAIF γ rays (Fultz 1966 and Veyssiere 1974) are indicated by squares and diamonds, respectively.

First, the measured cross sections for the ^{27}Al(γ, n)^{26}Al reaction are compared with TENDL-2021 [38] and the available experiments from various γ ray sources. In Fig.7, the data from Baglin [39] and Mutsuro [40], originate from gamma sources induced by the bremsstrahlung beam γ, while the data from Fultz [41] and Veyssiere [42] are derived from gamma sources associated with PAIF. It can be visually discerned that there are distinct segmented characteristics in the differences among the data sets.

The uncertainty of the specific data is shown as the measured data in the energy region below 16.3 MeV are in high agreement with the data obtained by Fultz using the PAIF

gamma source. In the energy region above 16.3 MeV, the measured data is significantly higher than the data obtained by Fultz and Veyssiere using PAIF γ sources, but agrees with the data obtained by Biglin *et al* using bremsstrahlung γ sources. With respect to the global structure of the data, this work set shows high consistency with the TENDL-2021 [38] data and exhibits a more uniform smoothness, whereas the Fultz and Veyssiere datasets display multiple oscillations during the increased cross section. These oscillations show poorer agreement with the calculations from relevant nuclear reaction models, such as the quasiparticle random phase approximation (QRPA) [43], and the oscillations are particularly pronounced during the ascent of the QRPA ^{27}Al(γ, n)^{26}Al cross section. The implications of this work are significant for both the evaluation of nuclear data and the optimization of the parameters of the theoretical model.

As discussed in Ref. [44], the ratios of the integral cross sections provide a clear indication of the systematic differences among the various data compilations. The integral cross sections in the S$_n$ and S$_{max}$ regions are as follows:

$$\sigma^{int} = \int_{S_n}^{S_{max}} \sigma(E)dE. \tag{7}$$

Experiments for the reactions ^{197}Au(γ, n) and ^{159}Tb(γ, n) reactions have been performed in SLEGS [32]. A comparison of the ^{197}Au(γ, n) reaction data with the findings of Itoh *et al* [35]. reveals a resulting integrated cross section difference of approximately 0.4%, which underscores the reliability of SLEGS in both measurement procedures and data analysis. Based on these reliable experimental data, the integral ratios of the photoneutron cross section were calculated for energy ranges from S$_n$ to 16.3 MeV, 16.3 MeV to E$_{max}$ and S$_n$ to E$_{max}$, as shown in Table 2. In the energy range of S$_n$ to 16.3 MeV, the experimental results in this work differ from the Fultz data only by 4%, while the discrepancy with other datasets exceeds 30%. In the energy range from 16.3 MeV to E$_{max}$, the results in this work show a difference of 3% compared to Bagin's results and by 4% from TENDL, with discrepancies from other datasets ranging between 8% and 28%. In general, the TENDL evaluated data agree with the measured data in this work across the energy range from 13 to 20 MeV, but the fast decrease after 20 MeV is not physically reasonable. The differences between the data in this measurement and those in other laboratories range from 3% to 25%. In particular, after the energy exceeds 20 MeV, due to the relatively large energy intervals between the TENDL data points and the unusually rapid decline in the high-energy segment, the differences between TENDL and the data from other laboratories become more pronounced. The rise of the cross section in this work is smooth, with no resonance structure peaks observed. Therefore, it is speculated that the resonance structures measured in other laboratories might be an artifact arising from the process of solving for single-energy cross sections. Considering the variations in data structure between the measured results, these data have significant implications for both the refinement of nuclear data evaluations and the optimization of the theoretical model parameters, as well as for resolving the discrepancies in the ^{27}Al(γ, n)^{26}Al reaction cross section and improving the understanding of its underlying nuclear structure.

Table 2. Integral cross section ratio.

Ratio relation	σ^{int}ratio		
	S$_n$-16.3MeV	16.3-E$_{max}$	S$_n$-E$_{max}$
$\sigma^{int}_{\text{TENDL}}/\sigma^{int}_{\text{SLEGS}}$	1.46	0.96	0.99
$\sigma^{int}_{\text{Baglin}}/\sigma^{int}_{\text{SLEGS}}$	1.36	1.03	1.11
$\sigma^{int}_{\text{Mutsuro}}/\sigma^{int}_{\text{SLEGS}}$	1.63	0.92	0.97
$\sigma^{int}_{\text{Fultz}}/\sigma^{int}_{\text{SLEGS}}$	1.04	0.72	0.74
$\sigma^{int}_{\text{Veyssiere}}/\sigma^{int}_{\text{SLEGS}}$	0.69	0.77	0.75

IV. SUMMARY

Measurements of cross sections for the ^{27}Al(γ, n)^{26}Al reactions were conducted from an incident energy of 13.2 to 21.7 MeV using the ^{3}He FED system developed by SLEGS. The precision of these measurements is highlighted by an overall uncertainty margin that is carefully maintained below 4%. Through careful data deviation and ratio analyses, a comprehensive comparison has been made between current photoneutron cross-sectional data and previous datasets, facilitating the resolution of discrepancies within the ^{27}Al photonuclear cross-sectional data and simultaneously refining the relevant theoretical models. Recognizing the critical role of the ^{27}Al photoneutron cross section in aerospace and astrophysics applications, we commit ourselves to extending the energy range of future investigations. This expansion will include a more thorough examination of both the ^{27}Al(γ, n)^{26}Al cross section and the ^{27}Al(γ, 2n)^{25}Al cross section.

V. ACKNOWLEDGEMENT

The authors thank the SSRF team for their stable maintenance of the electron beam during the experiments. The authors also thank Professor Yifei Niu (Lanzhou U.), Danyang Pang (Beihang U.) and Chuangye He (CIAE, China) for useful discussions.

[1] S. S. Dietrich, B. L. Berman, Atlas of photoneutron cross sections obtained with monoenergetic photons, Tech. Rep., Univ. of California, Livermore, **38**, 199 (1988). doi:10.1016/0092-640X(88)90033-2.

[2] M. Chadwick, P. Oblozinsky, A. Blokhin *et al.*, Handbook on photonuclear data for applications: Cross sections and spectra,

IAEA Tech-Doc **1178**, (2000).

[3] P. Mohr, K. Vogt, M. Babilon *et al.*, Experimental simulation of a stellar photon bath by bremsstrahlung: the astrophysical γ-process, Phys. Lett. B **488**, 127 (2000). doi:10.1016/S0370-2693(00)00862-5.

[4] D. Savran, T. Aumann, A. Zilges, Experimental studies of the pygmy dipole resonance, Prog. Part. Nucl. Phys. **70**, 210 (2013). doi:10.1016/j.ppnp.2013.02.003.

[5] B. L. Berman, S. Fultz, Measurements of the giant dipole resonance with monoenergetic photons, Rev. Mod. Phys. **47**, 713 (1975). doi:10.1103/RevModPhys.47.713.

[6] H. K. Wu, X. Y. Wang, Y. M. Wang *et al.*, Fudan multipurpose active target time projection chamber (fMeta-TPC) for photonuclear reaction experiments, Nucl. Sci. Tech. **35**, 200 (2024). doi:10.1007/s41365-024-01576-1.

[7] H. Ohgaki, S. Sugiyama, T. Yamazaki *et al.*, Measurement of laser-induced Compton backscattered photons with anti-Compton spectrometer, IEEE T. Nucl. Sci. **38**, 386 (1991). doi:10.1109/23.289330.

[8] G. Matthieu, The abundance of ^{26}Al-rich planetary systems in the Galaxy, Astronomy & Astrophysics **582**, A26 (2015). 10.1051/0004-6361/201526174.

[9] H. Utsunomiya, S. Goriely, T. Kondo *et al.*, Photoneutron cross sections for Mo isotopes: A step toward a unified understanding of (γ, n) and (n, γ) reactions, Phys. Rev. C **88**, 015805 (2013). doi:10.1103/PhysRevC.88.015805.

[10] C. Angell, S. Hammond, H. Karwowski *et al.*, Evidence for radiative coupling of the pygmy dipole resonance to excited states, Phys. Rev. C **86**, 051302 (2012). doi:10.1103/PhysRevC.86.051302.

[11] T. Kondo, H. Utsunomiya, S. Goriely *et al.*, Total and partial photoneutron cross sections for Pb isotopes, Phys. Rev. C **86**, 014316 (2012). doi:10.1103/PhysRevC.86.014316.

[12] I. Gheorghe, H. Utsunomiya, S. Katayama *et al.*, Photoneutron cross-section measurements in the ^{209}Bi(γ, xn) reaction with a new method of direct neutron-multiplicity sorting, Phys. Rev. C **96**, 044604 (2017). doi:10.1103/PhysRevC.96.044604.

[13] M. Krzysiek, H. Utsunomiya, I. Gheorghe *et al.*, Photoneutron cross-section measurements for ^{165}Ho by the direct neutron-multiplicity sorting at NewSUBARU, Acta Phys. Pol. B **50**, 487 (2019). doi:10.5506/aphyspolb.50.487.

[14] I. Gheorghe, H. Utsunomiya, K. Stopani *et al.*, Updated neutron-multiplicity sorting method for producing photoneutron average energies and resolving multiple firing events, Nucl. Instrum. Meth. A **1019**, 165867 (2021). doi:10.1016/j.nima.2021.165867.

[15] A. Banu, J. Silano, H. Karwowski *et al.*, Cross-section measurements of the ^{94}Mo(γ, n) and ^{90}Zr(γ, n) reactions using real photons at the HIγS facility, EPJ Web of Conferences **178**, 03007 (2018). doi:10.1051/epjconf/201817803007.

[16] A. Banu, E. Meekins, J. Silano *et al.*, Photoneutron reaction cross section measurements on ^{94}Mo and ^{90}Zr relevant to the p-process nucleosynthesis, Phys. Rev. C **99**, 025802 (2019). doi:10.1103/PhysRevC.99.025802.

[17] H. Y. Lan, D. Wu, J. X. Liu *et al.*, Photonuclear production of nuclear isomers using bremsstrahlung induced by laser-wakefield electrons, Nucl. Sci. Tech. **34**, 74 (2023). doi:10.1007/s41365-023-01219-x.

[18] W. Luo, Production of medical radioisotope ^{64}Cu by photoneutron reaction using ELI-NP γ-ray beam, Nucl. Sci. Tech. **27**, 96 (2016). doi:10.1007/s41365-016-0094-6.

[19] B. Ishkhanov, V. Varlamov, Photonuclear reactions: Modern status of the data, Phys. At. Nucl. **67**, 1664 (2004). doi:10.1134/1.1806905.

[20] H. W. Wang, G. T. Fan, L. X. Liu *et al.*, Commissioning of laser electron gamma beamline SLEGS at SSRF, Nucl. Sci. Tech. **33**, 87 (2022). doi:10.1007/s41365-022-01076-0.

[21] Z. R. Hao, G. T. Fan, H. W. Wang *et al.*, Collimator system of SLEGS beamline at Shanghai Light Source, Nucl. Instrum. Meth. A **1013**, 165638 (2021). doi:10.1016/j.nima.2021.165638.

[22] H. H. Xu, G. T. Fan, H. W. Wang *et al.*, Interaction chamber for laser Compton slant-scattering in SLEGS beamline at Shanghai Light Source, Nucl. Instrum. Meth. A **1033**, 166742 (2022). doi:10.1016/j.nima.2022.166742.

[23] L. X. Liu, H. W. Wang, G. T. Fan *et al.*, The SLEGS beamline of SSRF, Nucl. Sci. Tech. **35**, 111 (2024). doi:10.1007/s41365-024-01469-3.

[24] Z. R. Hao, H. H. Xu, G. T. Fan *et al.*, Gamma spot monitor at SLEGS beamline, Nucl. Instrum. Meth. A **1068**, 169748 (2024). doi:10.1016/j.nima.2024.169748.

[25] Z. C. Li, Y. Yang, Z. W. Cao *et al.*, Effective extraction of photoneutron cross-section distribution using gamma activation and reaction yield ratio method, Nucl. Sci. Tech. **34**, 170 (2023). doi:10.1007/s41365-023-01330-z.

[26] X. Pang, B. H. Sun, L. H. Zhu *et al.*, Progress of photonuclear cross sections for medical radioisotope production at the SLEGS energy domain, Nucl. Sci. Tech. **34**, 187 (2023). doi:10.1007/s41365-023-01339-4.

[27] S. Amano, K. Horikawa, K. Ishihara *et al.*, Several-MeV γ rays generation at NewSUBARU by laser Compton backscattering, Nucl. Instrum. Meth. A **602**, 337 (2009). doi:10.1016/j.nima.2009.01.010.

[28] L. X. Liu, H. Utsunomiya, G. T. Fan *et al.*, Energy profile of laser Compton slant-scattering γ-ray beams determined by direct unfolding of total-energy responses of a BGO detector, Nucl. Instrum. Meth. A **1063**, 169314 (2024). doi:10.1016/j.nima.2024.169314.

[29] W. Luo, H. Y. Lan, Y. Xu *et al.*, Implementation of the n-body Monte-Carlo event generator into the Geant4 toolkit for photonuclear studies, Nucl. Instrum. Meth. A **849**, 49 (2017). doi:10.1016/j.nima.2017.01.010.

[30] S. Agostinelli, J. Allison, K. A. Amako *et al.*, Geant4—a simulation toolkit, Nucl. Instrum. Meth. A **506**, 250 (2003). doi:10.1016/S0168-9002(03)01368-8.

[31] W. Luo, D. L. Balabanski, D. Filipescu, A data-based photonuclear simulation algorithm for determining specific activity of medical radioisotopes, Nucl. Sci. Tech. **27**, 113 (2016). doi:10.1007/s41365-016-0111-9.

[32] Z. R. Hao, G. T. Fan, H. W. Wang *et al.*, Systematic measurement of the (γ, 1n) cross sections on ^{197}Au and ^{159}Tb, Science Bulletin (Submitted).

[33] Z. R. Hao, G. T. Fan, L. X. Liu *et al.*, Design and simulation of 4π flat-efficiency ^{3}He neutron detector array, Nucl. Tech. (in Chinese) **43**, 9 (2020). doi:10.11889/j.0253-3219.2020.hjs.43.110501.

[34] B. Berman, J. Caldwell, R. Harvey *et al.*, Photoneutron cross sections for ^{90}Zr, ^{91}Zr, ^{92}Zr, ^{94}Zr, and ^{89}Y, Phys. Rev. **162**, 1098 (1967). doi:10.1103/PhysRev.162.1098.

[35] O. Itoh, H. Utsunomiya, H. Akimune *et al.*, Photoneutron cross sections for Au revisited: measurements with laser Compton scattering γ-rays and data reduction by a least-squares method, J. Nucl. Sci. Technol. **48**, 834 (2011). doi:10.1080/18811248.2011.9711766.

[36] T. Renstrøm, H. Utsunomiya, H. T. Nyhus *et al.*, Verification of detailed balance for γ absorption and emis-

sion in Dy isotopes, Phys. Rev. C **98**, 054310 (2018). doi:10.1103/PhysRevC.98.054310.

[37] G. C. Yang, L. M. Hua, F. Lu *et al.*, Response functions of a 4 π summing gamma detector in β-Olso method, Nucl. Sci. Tech. **33**, 68 (2022). doi:10.1007/s41365-022-01058-2

[38] TENDL-2021, `https://tendl.web.psi.ch/tendl_2021/gamma_html/gamma.html`, (2021).

[39] J. Baglin, M. Thompson, B. Spicer, Photodisintegration of ^{27}Al:(I) photoneutron cross section, Nucl. Phys. **22**, 207 (1961). doi:10.1016/0029-5582(61)90453-9.

[40] N. Mutsuro, K. Kageyama, M. Mishina *et al.*, Structure of giant resonance in ^{27}Al (γ,n) reaction, J. Phys. Soc. Japan **17**, 1672 (1962). doi:10.1143/JPSJ.17.1672.

[41] S. Fultz, J. Caldwell, B. Berman *et al.*, Photoneutron cross sections for ^{12}C and ^{27}Al, Phys. Rev. **143**, 790 (1966). doi:10.1103/PhysRev.143.790.

[42] A. Veyssiere, H. Beil, R. Bergere *et al.*, A study of the photoneutron contribution to the giant dipole resonance of sd shell nuclei, Nucl. Phys. A **227**, 513 (1974). doi:10.1016/0375-9474(74)90774-X.

[43] Z. Z. Li, Y. F. Niu, G. Colò, Toward a unified description of isoscalar giant monopole resonances in a self-consistent quasiparticle-vibration coupling approach, Phys. Rev. Lett. **131**, 082501 (2023). doi:10.1103/PhysRevLett.131.082501.

[44] V. Varlamov, B. Ishkhanov, V. Orlin, Reliability of (γ, 1n),(γ, 2n), and (γ, 3n) cross-section data on ^{159}Tb, Phys. Rev. C **95**, 054607 (2017). doi:10.1103/PhysRevC.95.054607.